JACS
JOURNAL OF THE AMERICAN CHEMICAL SOCIETY
Article
pubs.acs.org/JACS

Chalcogenophene Comonomer Comparison in Small Band Gap Diketopyrrolopyrrole-Based Conjugated Polymers for High-Performing Field-Effect Transistors and Organic Solar Cells

Raja Shahid Ashraf,*[,†] Iain Meager,*[,†] Mark Nikolka,[§] Mindaugas Kirkus,[†] Miquel Planells,[†] Bob C. Schroeder,[†] Sarah Holliday,[†] Michael Hurhangee,[†] Christian B. Nielsen,[†] Henning Sirringhaus,[§] and Iain McCulloch[†,‡]

[†]Department of Chemistry and Centre for Plastic Electronics, Imperial College London, London SW7 2AZ, United Kindgom
[‡]Physical Sciences and Engineering Division, King Abdullah University of Science and Technology (KAUST), Thuwal, 23955−6900, Saudi Arabia
[§]Cavendish Laboratory, University of Cambridge, Cambridge, CB3 0HE, United Kindgom

Supporting Information

ABSTRACT: The design, synthesis, and characterization of a series of diketopyrrolopyrrole-based copolymers with different chalcogenophene comonomers (thiophene, selenophene, and tellurophene) for use in field-effect transistors and organic photovoltaic devices are reported. The effect of the heteroatom substitution on the optical, electrochemical, and photovoltaic properties and charge carrier mobilities of these polymers is discussed. The results indicate that by increasing the size of the chalcogen atom (S < Se < Te), polymer band gaps are narrowed mainly due to LUMO energy level stabilization. In addition, the larger heteroatomic size also increases intermolecular heteroatom−heteroatom interactions facilitating the formation of polymer aggregates leading to enhanced field-effect mobilities of 1.6 $cm^2/(V\ s)$. Bulk heterojunction solar cells based on the chalcogenophene polymer series blended with fullerene derivatives show good photovoltaic properties, with power conversion efficiencies ranging from 7.1−8.8%. A high photoresponse in the near-infrared (NIR) region with excellent photocurrents above 20 mA cm^{-2} was achieved for all polymers, making these highly efficient low band gap polymers promising candidates for use in tandem solar cells.

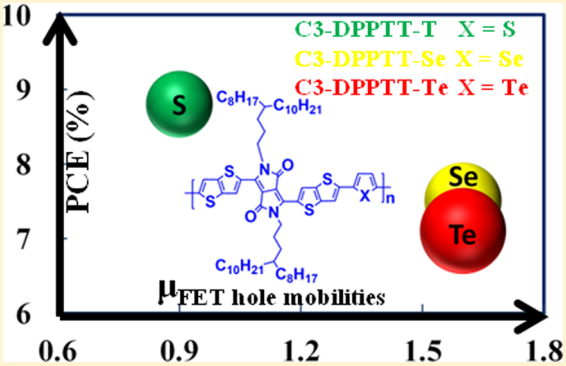

INTRODUCTION

In the development of highly efficient organic field-effect transistor (OFET) and photovoltaic (OPV) devices the diversity in design of conjugated polymers continues to accelerate, with an ongoing strive toward novel structures.[1−3] Conjugated polymer backbones containing alternating electron-rich donor and electron-poor acceptor units have emerged as a popular approach in the design of low band gap materials.[4] By careful consideration of the repeating donor and acceptor units, control over the highest occupied molecular orbital (HOMO) and lowest unoccupied molecular orbital (LUMO) energy levels of these polymers is possible.[5] This facilitates the design of a variety of chromophores with optimal light absorption properties for OPV applications and energy level alignment for the injection and extraction of charges in OFET devices.[4−8] To date, some of the highest performing polymers for organic electronic applications utilize this concept.[6,9−13] Of these high-performing materials, diketopyrrolopyrrole (DPP) is one of the most versatile and widely used structural motifs.[6] The bis-lactam core results in off-axis dipoles along the polymer backbone which have been known to facilitate increased intermolecular interactions, while the fused nature of the DPP unit has low conformational disorder leading to highly coplanar polymer chains.[14] The lactam nitrogens of the DPP core provide a fairly straightforward route toward alkylation which is essential for polymer solubility.[15] Copolymerization of the electron-deficient DPP unit, flanked by thiophene (**DPPT**) or thieno[3,2-*b*]thiophene (**DPPTT**), with other heterocyclic units has previously led to a variety of narrow band gap semiconducting copolymers with good OPV and OFET device performances.[15−25] Of these heterocycles, group VI chalcogen-based units remain relatively unexplored. While a number of examples of selenophene and tellurophene substitution can be found in the literature, a comprehensive understanding of the effect that chalcogen heteroatom variation has on polymer optical and physical properties as well as OPV and OFET performance is elusive, with only one study of a series of low

Received: November 23, 2014
Published: December 29, 2014

DOI: 10.1021/ja511984q
J. Am. Chem. Soc. 2015, 137, 1314−1321

band gap isoindigo polymers containing thiophene, selenophene and tellurophene.[26] Descending the group from thiophene to tellurophene is known to correspond to a reduction in chalcogenophene aromaticity.[26−28] This is a result of larger heteroatomic size, which leads to poor orbital overlap between the heteroatom and the π-system located on the carbon atoms. This results in increased quinoidal contribution, which gives increased double-bond character and decreased bond lengths for the inter ring C−C bonds. Due to the shorter C−C bonds for the larger/heavier chalcogenophenes compared to thiophene, it is expected that the quinoid structure will make a significantly larger contribution to the molecular orbital energy levels, leading to a red-shift in the absorption profile of the resultant copolymers. The heavier chalcogen heteroatoms (Se and Te) also have lower electronegativity (2.4 and 2.1, respectively) than sulfur (2.5).[29] Tellurium has the lowest electronegativity of the three resulting in carbon−tellurium bonds that are inversely polarized $Te^{\delta+}-C^{\delta-}$, while the larger and more polarizable radii of both selenium and tellurium heteroatoms are expected to lead to stronger intermolecular interactions.[30−32] These stronger intermolecular interactions in selenium- and tellurium-containing copolymers are likely to result in increased overlap of π-electrons, which is known to be beneficial for charge transport.[19,21,22,26−28,33]

DPPTT has previously been shown by our group to be one of the most promising DPP derivatives reported to date, with impressive performances observed in both OPV and OFET devices.[15,23,34] We have also demonstrated that moving the branching point of alkyl chains further from the **DPPTT** backbone leads to an enhancement in device performances due to increased intermolecular association and improved solubility.[15] Consequently, the **C3-DPPTT** monomer unit (where C3 refers to the number of linear carbon atoms between the alkylated nitrogen and the branched C_8H_{17} and $C_{10}H_{21}$ alkyl chains) was chosen for further work due to its potential to facilitate high OPV performance, high hole mobilities, and superior solution processability. Copolymers of this **C3-DPPTT** unit with chalcogenophene comonomers of increasing heteroatom size (Te > Se > S) were synthesized, and the effect of the heavy atom substitution on optical, physical and device properties are investigated in detail.

RESULTS AND DISCUSSION

The synthesis of all three polymers is shown in Scheme 1, and the synthetic procedures are described in the Supporting Information (SI). The dibrominated **C3-DPPTT** monomer was copolymerized with bis-stannylated thiophene, selenophene, and tellurophene comonomers using microwave-assisted palladium-catalyzed Stille coupling in chlorobenzene to afford polymers **C3-DPPTT-T**, **C3-DPPTT-Se**, and **C3-DPPTT-Te**, respectively.[15,35−38] Purification of the crude polymers was carried out by Soxhlet extraction in acetone, hexane, and chloroform. The chloroform fraction was treated with diethyldithiocarbamic acid diethylammonium salt to remove any residual palladium catalyst. All three comonomers afforded high number average molecular weight (M_n) polymers with relatively narrow dispersity (Đ) (Table 1).

Scheme 1. Synthesis of Polymers by Palladium-Catalyzed Stille Coupling

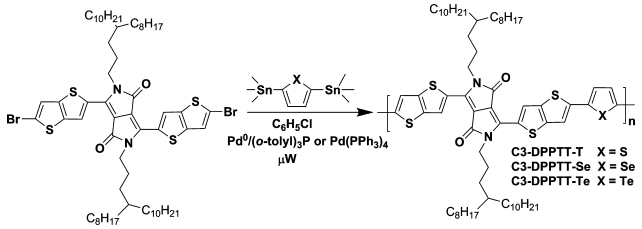

Table 1. Molecular Weight Properties of Polymers C3-DPPTT-T, C3-DPPTT-Se, and C3-DPPTT-Te

polymer	M_n (kDa)[a]	M_w (kDa)[a]	Đ[a]	DP_n[a]
C3-DPPTT-T	80	154	1.9	72.0
C3-DPPTT-Se	95	238	2.5	82.0
C3-DPPTT-Te	91	272	3.0	75.4

[a] M_n, M_w, Đ (M_w/M_n), and DP_n (M_n/M_0) determined by gel permeation chromatography (GPC) using low-Đ (<1.10) polystyrene standards and chlorobenzene as the eluent at 80 °C.

The effect of heteroatom substitution is clearly observable in the UV−vis absorption profiles of the three copolymers (Figure 1). As expected, **C3-DPPTT-Se** and **C3-DPPTT-Te** showed a red-shift in the absorption profile and a narrowing of optical band gaps (E_g) compared to **C3-DPPTT-T** which is likely a consequence of the larger heteroatoms. The solution absorption maxima (λ_{max}) increases from 804 nm with **C3-DPPTT-T** to 832 nm with **C3-DPPTT-Se**, while a similar trend is observed in the thin film profiles going from 803 nm for **C3-DPPTT-T** to 831 nm for **C3-DPPTT-Se**. **C3-DPPTT-Te** shows the most red-shifted absorption spectra with λ_{max} of 866 nm both in solution and thin film and a band gap of 1.32 eV (Table 2). In addition to the variation of λ_{max}, it can also be seen from the UV−vis absorption spectra that increased heteroatomic size corresponds to an increase in solution aggregation based upon the relative intensities of the two dominant absorption features.

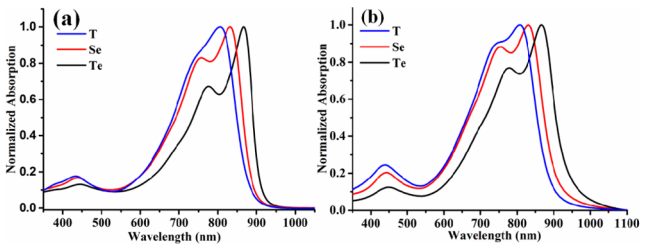

Figure 1. UV−vis absorption profiles of polymers **C3-DPPTT-T**, **C3-DPPTT-Se**, and **C3-DPPTT-Te** (a) in dilute chlorobenzene solution and (b) as thin films spin coated on glass substrates from 5 mg/mL chlorobenzene solution.

To further examine each polymer's tendency for aggregation, temperature-dependent UV−vis absorption spectra of dilute chlorobenzene solutions of **C3-DPPTT-T**, **C3-DPPTT-Se**, and **C3-DPPTT-Te** were recorded at increasing temperature intervals of 10 °C (Figure 2).

The absorption profile of the thiophene-containing polymer **C3-DPPTT-T** shows a shift to an almost entirely Gaussian shape at 85 °C, with the small absorption shoulder that is present at room temperature disappearing at elevated temperatures, indicating that aggregates are almost fully dissociated. Although not as dramatic, the selenophene-containing copolymer **C3-DPPTT-Se** shows a similar trend with a longer

DOI: 10.1021/ja511984q
J. Am. Chem. Soc. 2015, 137, 1314−1321

Table 2. Optical and Electrochemical Properties of Polymers C3-DPPTT-T, C3-DPPTT-Se, and C3-DPPTT-Te

	λ_{max} (nm)		measured			calculated		
polymer	solution[a]	film[b]	E_{HOMO} (eV)[c]	E_{LUMO} (eV)[d]	E_g (eV)[e]	E_{HOMO} (eV)[f]	E_{LUMO} (eV)[f]	E_g (eV)[f]
C3-DPPTT-T	803	804	−5.08	−3.69	1.39	−4.97	−3.15	1.82
C3-DPPTT-Se	831	832	−5.07	−3.70	1.37	−4.96	−3.20	1.76
C3-DPPTT-Te	866	866	−5.05	−3.73	1.32	−4.95	−3.21	1.74

[a]Dilute chlorobenzene solution. [b]Spin coated from 5 mg/mL chlorobenzene solution. [c]HOMO levels (E_{HOMO}) estimated using PESA. [d]Estimated by adding E_g to E_{HOMO}. [e]Estimated from the UV−vis onset of absorption. [f]Calculated using TD/DFT calculations with B3LYP/6-311G(d) (H, C, S, N, O atoms) and SDD ECP (Se, Te atoms) basis sets.

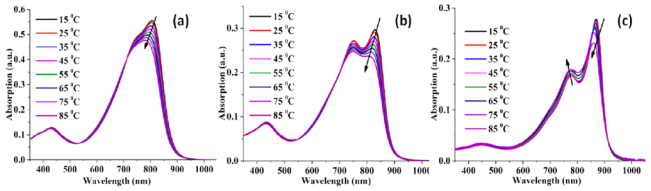

Figure 2. Temperature-dependent UV−vis absorption profiles in dilute chlorobenzene solution for (a) **C3-DPPTT-T**, (b) **C3-DPPTT-Se**, and (c) **C3-DPPTT-Te**.

wavelength shoulder that is significantly reduced at higher temperatures. However, for **C3-DPPTT-Te** there remains a significant absorption shoulder indicating the presence of polymer aggregates even at elevated temperatures. This increased tendency for solution aggregation of polymers with larger heteroatomic size is likely a consequence of stronger intermolecular interactions between larger chalcogen atoms as group VI is descended.

The frontier molecular orbital energies, E_{HOMO} and E_{LUMO}, were estimated using photoelectron spectroscopy in air (PESA) and UV−vis absorption onsets, respectively. The increasing heteroatom size of the chalcogenophene comonomer leads to a small but consistent raising of E_{HOMO}. **C3-DPPTT-T** can be seen to have the deepest lying value of −5.08 eV, **C3-DPPTT-Se** has a slightly raised value of −5.07 eV, while a further increase in chalcogen size to tellurophene sees the highest E_{HOMO} value of −5.05 eV for **C3-DPPTT-Te**. A similar magnitude stabilization of E_{LUMO} values is also observed with increasing chalcogen size. These small but observable trends are consistent with our group's very recently published chalcogen study on cyclopentadithiophene (**CPDT**)-based polymers as well as DFT calculations discussed in the next section.[39]

In order to further understand the effect of chalcogen atoms on optical and electrochemical properties of these polymers, hybrid DFT calculations were performed on trimeric systems in vacuum using a B3LYP/6-311G(d) level of theory. To describe the heavy atoms selenium and tellurium, Stuttgart−Dresden (SDD) effective core potentials (ECP) were used. The predicted absorption profiles of the three polymers (Figure S1) closely match the experimentally determined trend, with the exception of the size of the longer wavelength absorption shoulder due to computational results not accounting for aggregation effects.

DFT predicted frontier molecular orbital energy levels and spatial distributions for the chalcogen series are shown in Figure 3. Replacement of thiophene with selenophene and tellurophene only marginally raises E_{HOMO} values, while E_{LUMO} values are further stabilized, in good agreement with the experimental results (Table 2).

Computationally predicted energy-minimized polymer backbone structures are shown in Figure 3. Each of the three polymers demonstrates a highly planar backbone structure with a colinear long axis. All three polymers have evenly distributed HOMO electron densities with π character indicating good delocalization along the polymer backbone structures. There is minimal contribution of comonomer heteroatom to the HOMO wave function which is in good agreement with the small variation in E_{HOMO} values observed across the series. On the other hand, the LUMOs have a strong π^* character showing electron density delocalized over both the DPP and chalcogenophene units.

An X-ray diffraction (XRD) study on polymer thin films was carried out to evaluate how the differing intermolecular interactions relate to the microstructure of each polymer in the solid state. Figure 4 shows the diffractograms of the drop cast films of the three polymers. All three polymers exhibit a first-order (100) lamellar stacking peak at around 2θ = 4.2−4.4° corresponding to lamellar spacing distances of approximately 20−21 Å. Expectedly the heavy atom substitution does not result in significant variation in these distances; the lamellar spacing appears to be governed by the long alkyl chains on the **DPPTT** unit which explains the lack of variation across the series. Both **C3-DPPTT-T** and **C3-DPPTT-Se** show a broad

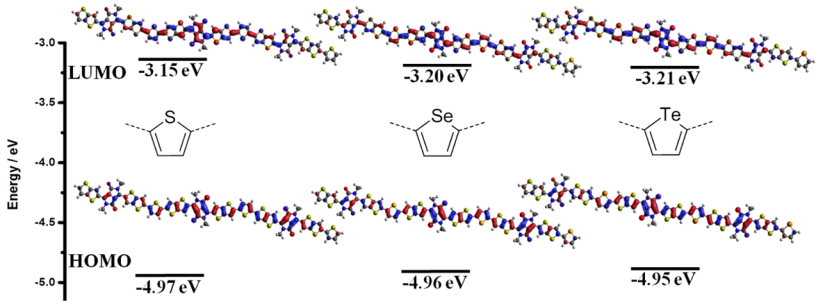

Figure 3. Predicted frontier molecular orbital distribution and energy levels at B3LYP/6-311G(d) (H, C, S, N, O atoms) and SDD ECP (Se, Te atoms) level of theory for **C3-DPPTT-T**, **C3-DPPTT-Se**, and **C3-DPPTT-Te** polymers. Isodensity = 0.02.

DOI: 10.1021/ja511984q
J. Am. Chem. Soc. 2015, 137, 1314−1321

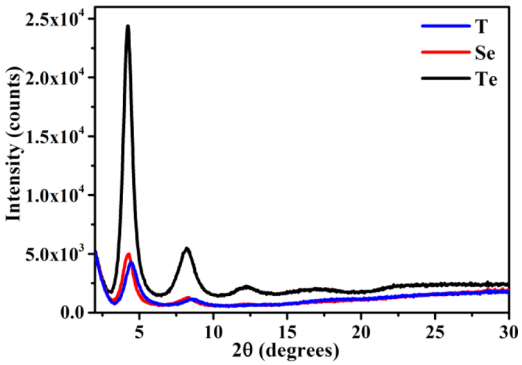

Figure 4. XRD diffractogram of **C3-DPPTT-T**, **C3-DPPTT-Se**, and **C3-DPPTT-Te** polymer films drop cast on Si wafers from 10 mg/mL chlorobenzene solution.

first-order peak of low intensity, whereas the same peak for **C3-DPPTT-Te** is more intense. From the full width at half-maximum (fwhm) values, average crystallite sizes on the order of 9−11 nm are estimated for all three films. A second-order (200) diffraction peak can also be seen for all three polymers, while in **C3-DPPTT-Te** there is an additional small third-order (300) reflection. The lack of diffraction peaks from π-stacking indicates that each polymer adopts a predominantly edge-on orientation relative to the substrate. Judging from each of the peak intensities, **C3-DPPTT-Te** appears to have a higher degree of edge-on crystallinity than the two other polymers in the series.

Annealing of the polymer films results in more intense and sharper diffraction peaks, indicating improved micro ordering (Figure S2). In general **C3-DPPTT-T** and **C3-DPPTT-Se** show approximately the same degree of crystallinity, while **C3-DPPTT-Te** is significantly more crystalline which is shown by the narrower and more intense reflection peaks. This is likely a consequence of the increased heteroatom−heteroatom interactions between tellurium atoms on adjacent polymer backbones compared to selenium or sulfur.

Figure 5a shows representative transfer characteristics of 20 μm long and 1 mm wide, low-temperature processed (100 °C) bottom-contact top-gate OFET devices comprising the polymers **C3-DPPTT-T**, **C3-DPPTT-Se**, and **C3-DPPTT-Te**. The transfer characteristics for all devices exhibit hysteresis-free behavior with high on currents between 0.2 and 0.4 mA. The high on-currents are reflected in saturation charge carrier mobilities (extracted at $V_{DS} = V_G = -80$ V) of 0.9 cm^2/(V s) for **C3-DPPTT-T** and 1.6 cm^2/(V s) for both **C3-DPPTT-Se** and **C3-DPPTT-Te** (Table 3). We were able to extract even higher mobilities for devices annealed at 200 and 300 °C, however these showed lower on-currents and less ideal performances and were hence discarded as artifacts. From the transfer characteristics shown in Figure 5a, it can furthermore be observed that devices comprising **C3-DPPTT-Se** and **C3-DPPTT-Te** exhibit a higher off-current and sub threshold slope as compared to devices fabricated from **C3-DPPTT-T**. We attribute this behavior to an increased susceptibility of **C3-DPPTT-Se** and **C3-DPPTT-Te** to oxygen which we noted after controlled exposure of the transistors to ambient air.

Table 3. OFET Properties of C3-DPPTT-T, C3-DPPTT-Se, and C3-DPPTT-Te in Devices with Bottom-Contact Top-Gate Architecture

polymer	μ_{hole} (cm^2 V^{-1} s^{-1})^a	V_{th} (V)^b	I_{on}/I_{off}^{b}
C3-DPPTT-T	0.9	−12	~1 × 10^3
C3-DPPTT-Se	1.6	−13	~1 × 10^3
C3-DPPTT-Te	1.6	−8	~1 × 10^3

^{a}Highest effective hole mobilities measured in the saturation regime. ^{b}Threshold voltages (V_{th}) and on/off ratios (I_{on}/I_{off}) extracted from the linear regime ($V_D = -5$ V).

In Figure 5b,c representative output characteristics and the gate voltage dependence of charge carrier mobility for the investigated polymers are presented. From the linear output characteristics measured for all three polymers, we conclude that there is no major contact resistance, and thus, device performances are not injection limited and extracted mobility values can therefore be considered accurate and representative. From the gate voltage dependence of extracted charge carrier mobilities we nevertheless note that extracted mobilities are gate voltage dependent, an effect which is amplified at higher gate voltages. This might partially be due to fringe currents as well as the filling of tail states in the polymer's density of states, an effect which can be observed in other semicrystalline polymer systems.[40]

Polymer/fullerene bulk heterojunction solar cells were fabricated with polymers **C3-DPPTT-T**, **C3-DPPTT-Se**, and **C3-DPPTT-Te** as the donor material to establish a relationship between chalcogen substitution within the DPP polymer series and OPV performance. An in depth investigation with both PC[60]BM and PC[70]BM fullerenes and device architecture variation was undertaken.

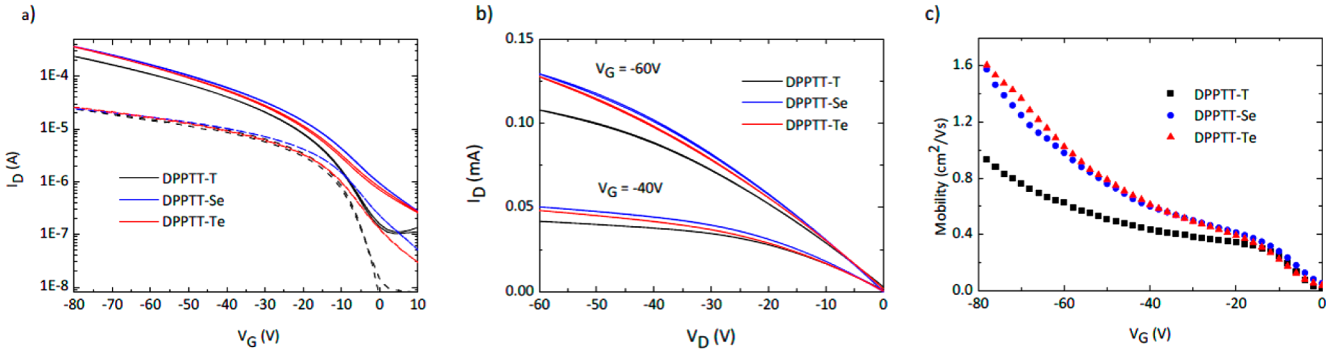

Figure 5. (a) Transfer characteristics, (b) output characteristics, and (c) gate-voltage dependence of saturation mobility for **C3-DPPTT-T**, **C3-DPPTT-Se**, and **C3-DPPTT-Te** OFETs ($L = 20$ μm, $W = 1$ mm). In the transfer curves dashed lines correspond to $V_D = -5$ V and solid lines to $V_D = -80$ V.

DOI: 10.1021/ja511984q
J. Am. Chem. Soc. 2015, 137, 1314−1321

Figures 6, 7, and 8 show the current−voltage (J−V) curves and external quantum efficiency (EQE) spectra with both

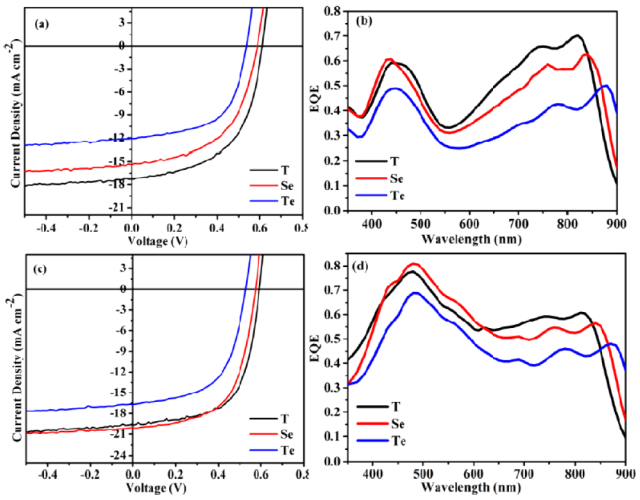

Figure 6. Polymer/PC[60]BM (a) J−V curve and (b) EQE spectra. Polymer/PC[70]BM (c) J−V curve and (d) EQE spectra for polymers **C3-DPPTT-T**, **C3-DPPTT-Se**, and **C3-DPPTT-Te** using conventional device architecture.

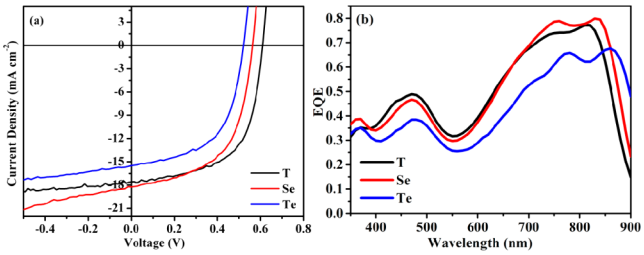

Figure 7. Polymer/PC[60]BM (a) J−V curve and (b) EQE spectra for polymers **C3-DPPTT-T**, **C3-DPPTT-Se**, and **C3-DPPTT-Te** using inverted device architecture.

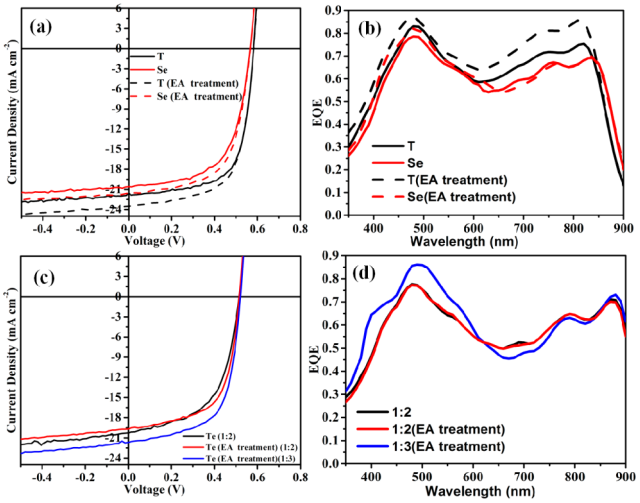

Figure 8. Polymer/PC[70]BM (a) J−V curve and (b) EQE spectra for polymers **C3-DPPTT-T** and **C3-DPPTT-Se**. (c) J−V curve and (d) EQE spectra of **C3-DPPTT-Te** using inverted device architecture with different blend ratios. (With and without use of 1% ethanolamine (EA) in 2-methoxyethanol.)

PC[60]BM and PC[70]BM using conventional and inverted device architecture, while Table 4 displays the respective performance parameters for each device.

The open circuit voltage (V_{oc}) of the cells of all three polymers follows a clear trend that is consistent with the E_{HOMO} values. **C3-DPPTT-T** shows the highest value of 0.61 V and **C3-DPPTT-Te** the lowest value of 0.53 V in conventional device architecture.

Each polymer shows high photocurrent values in PC[60]BM blend heterojunction, especially in the NIR(near-infrared) region with the **C3-DPPTT-T** blend yielding the highest short circuit current (J_{sc}) of 16.7 mA cm^{-2} and a power conversion efficiency (PCE) of 5.7%. Blends with **C3-DPPTT-Se** and **C3-DPPTT-Te** afford PCEs of 4.9% and 3.8%, respectively. The short circuit currents are further enhanced by the use of PC[70]BM as an acceptor as opposed to PC[60]BM. This substitution of fullerenes has previously been shown to be highly effective in increasing the photocurrent of the resultant devices due to the larger fullerene exhibiting a higher absorption coefficient. Each polymer in the series shows impressively high EQE (Figure 6) and a general increase in photocurrent over the entire spectrum is observed when PC[70]BM was used. As a consequence, PCE values are improved significantly with **C3-DPPTT-T** affording 7.0%, compared to 6.5% and 5.0% for C3-**DPPTT-Se** and **C3-DPPTT-Te** respectively.

Inverted devices were fabricated using the same photoactive layer but with ZnO employed as an electron transport layer and MoO_3 as the hole transport layer. Silver was preferred over aluminum as a back reflector. The optical electric field is enhanced in the inverted device architecture, resulting in more photon absorption leading to a better photoresponse.[41] Inverted architectures are also known to have improved interfacial contacts, which can lead to a more efficient charge collection and less electron−hole recombination.[42] The V_{oc} and J_{sc} values with both acceptors follow the same general trends as in the conventional architecture, with the highest values observed for **C3-DPPTT-T** and the lowest values for **C3-DPPTT-Te**. As expected, a photocurrent enhancement is observed with inversion of device architecture for each of the three polymers. This gives rise to a PCE increase from 5.7% to 6.5% for **C3-DPPTT-T** with PC[60]BM and similar improvements for the two other polymers in the series. Substitution of PC[60]BM with PC[70]BM again corresponds to an improvement in J_{sc} with values >20 mA cm^{-2} observed for all three polymers in the series. These J_{sc} values are among the highest reported for bulk heterojunction organic solar cells. Due to the higher V_{oc} and fill factor (FF), the thiophene copolymer gives an impressive PCE of 8.5%. The other two copolymers **C3-DPPTT-Se** and **C3-DPPTT-Te** likewise show high PCEs of about 7.0% and 5.9%, respectively.

Better device performance is observed in inverted solar cells, yet the FF of **C3-DPPTT-Te** is noticeably lower than the other chalcogenophene analogues. This could be a consequence of a large contact barrier between the active layer and cathode. Recently, many groups have shown different methods to improve the interface between the cathode and active layer.[43−46] In our case, interfacial modification of ZnO layer is performed by treatment with 1% ethanol amine (EA) in 2-methoxy ethanol.[46] As expected, an enhancement in PCE from 8.5 to 8.8 is observed for **C3-DPPTT-T** polymer. The other two polymers have also shown relatively higher PCEs of 7.6 and 6.3 for **C3-DPPTT-Se** and **C3-DPPTT-Te**, respectively

DOI: 10.1021/ja511984q
J. Am. Chem. Soc. 2015, 137, 1314−1321

Table 4. OPV Device Performance Characteristics of Polymers C3-DPPTT-T, C3-DPPTT-Se, and C3-DPPTT-Te with Both PC[60]BM and PC[70]BM Fullerene Acceptors (Polymer:Fullerene 1:2 w/w Blend Ratio) Using Conventional and Inverted Device Architectures

polymer	fullerene	device config.	J_{sc} (mA/cm^2)[a]	V_{oc} (V)	FF	PCE (%)[a]
C3-DPPTT-T	PC[60]BM	conventional	16.7	0.61	0.56	5.7
		inverted	17.6	0.61	0.61	6.5
C3-DPPTT-Se	PC[60]BM	conventional	15.5	0.59	0.54	4.9
		inverted	18.1	0.56	0.57	5.8
C3-DPPTT-Te	PC[60]BM	conventional	12.0	0.54	0.59	3.8
		inverted	15.5	0.52	0.57	4.6
C3-DPPTT-T	PC[70]BM	conventional	19.0	0.59	0.62	7.0
		inverted	21.5	0.58	0.68	8.5
		inverted[b]	23.5	0.57	0.66	8.8
C3-DPPTT-Se	PC[70]BM	conventional	19.1	0.57	0.60	6.5
		inverted	20.6	0.56	0.61	7.0
		inverted[b]	21.5	0.56	0.63	7.6
C3-DPPTT-Te	PC[70]BM	conventional	16.2	0.53	0.58	5.0
		inverted	20.2	0.52	0.56	5.9
		inverted[b]	19.7	0.52	0.62	6.3
		inverted (1:3)[b]	21.7	0.52	0.63	7.1

[a]EQE corrected. [b]Treatment of ZnO layer with 1% ethanol amine (EA) in 2-methoxyethanol.

(Figure 8, Table 4). The EA interfacial contact helps in reducing the contact and series resistance leading to higher PCEs. To further optimize the performance of **C3-DPPTT-Te**, polymer:PC[70]BM ratio is changed. The best performing devices are obtained with a 1:3 polymer:PC[70]BM weight ratio. For this optimized device the PCE is about 7.1% showing J_{sc} value of 21.7 mA cm^{-2}, V_{oc} is 0.52 and FF is 0.63(Figure 8, Table 4).

Distinct differences are noticeable when comparing the EQE spectra of the inverted devices (Figure 7) with those of the conventional devices. In inverted devices, at longer wavelengths EQE responses were increased by about 10% due to the enhanced absorption. This gives an effective increase of between 1 and 4 mA cm^{-2} in the short-circuit current. In the case of **C3-DPPTT-Te** the photoresponse was extended beyond 900 nm, with a 35% EQE at 900 nm, making it a promising candidate material for multijunction organic solar cells.

Atomic force microscopy (AFM) was used to investigate the surface morphologies of the polymer:fullerene blends (Figure 9). A homogeneous film is observed for each blend, and there are no distinct variations in nanoscale morphology. **C3-DPPTT-Te** blends exhibit slightly coarser morphologies, which is supported by the increased root-mean-square (RMS) surface roughness (Figure 8). A noticeable difference between the blend morphologies of both types of device is that inverted devices exhibit observably larger domain sizes. It has been observed experimentally that the use of different material interlayers in OPV devices can not only modify electrode work function but also result in a wide range of blend morphologies due to the changing surface energies of these interfacial layers.[47,48] Despite these small changes, it is likely that previously observed variations in light absorption and energy level alignments are more significant contributors to the different solar cell device performances than any minor blend morphology effects.

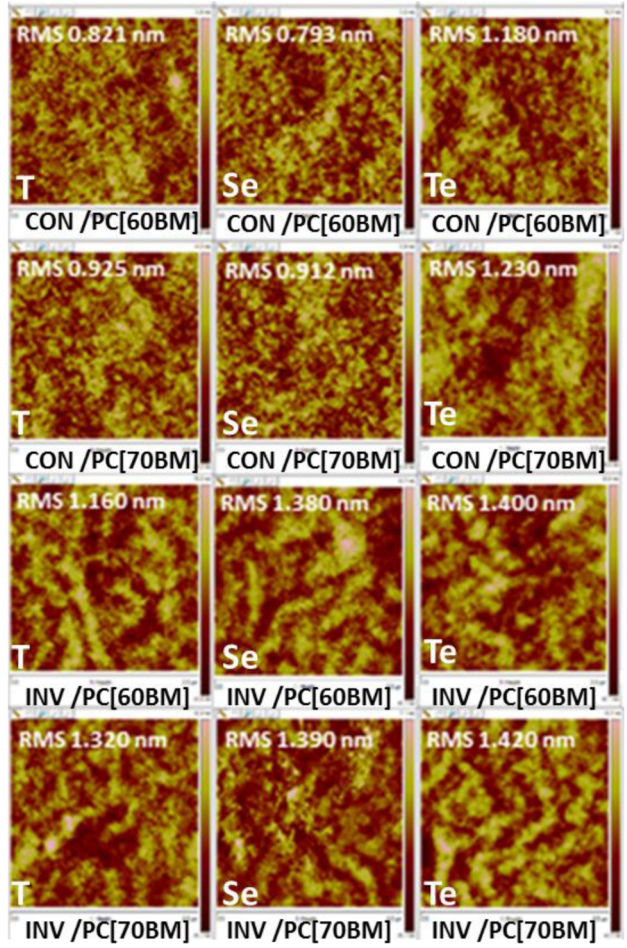

Figure 9. AFM topography images of polymers **C3-DPPTT-T**, **C3-DPPTT-Se**, and **C3-DPPTT-Te** conventional (CON)/inverted (INV) device architectures with both PC[60]BM and PC[70]BM fullerene acceptors.

CONCLUSIONS

In this study we report the synthesis of a series of **C3-DPPTT** copolymers with chalcogenophene comonomer units of increasing heteroatomic size (thiophene, selenophene, and tellurophene). The two new copolymers are compared

DOI: 10.1021/ja511984q
J. Am. Chem. Soc. 2015, 137, 1314−1321

computationally and experimentally with the previously reported thiophene copolymer **C3-DPPTT-T**. With an increase in chalcogen atomic size, a reduction in aromaticity causes a slight raise in E_{HOMO} values and decrease in E_{LUMO} values which results in a narrowing of optical band gaps and a red-shifting of UV−vis absorption profiles. XRD analysis shows that the size of chalcogen atom can significantly influence the crystallinity of the neat polymer films. The heavier chalcogen atoms, selenium and tellurium, with higher polarizability and stronger intermolecular interactions in the solid state lead to enhanced field-effect hole mobilities of 1.6 $cm^2/(V\ s)$ in **C3-DPPTT-Se** and **C3-DPPTT-Te** copolymers. Comparison of the three chalcogenophene polymers with differing fullerene acceptors and photovoltaic device architectures shows a decrease in V_{oc} with increasing heteroatom size. Despite these reductions, high-performing solar cells were obtained with efficiencies as high as 8.8% for thiophene, 7.6% for selenophene, and 7.1% for tellurophene.

The device performance of **C3-DPPTT-T** is the highest reported for a DPP-based polymer in a single junction device, while to the best of our knowledge the selenophene and tellurophene copolymers give the highest performing OPV devices reported for each of the respective heterocycles.

■ ASSOCIATED CONTENT

Supporting Information

Experimental details, synthesis and analysis of the polymers, and additional figures. This material is available free of charge via the Internet at http://pubs.acs.org.

■ AUTHOR INFORMATION

Corresponding Authors

*r.ashraf@imperial.ac.uk

*i.meager11@imperial.ac.uk

Notes

The authors declare no competing financial interest.

■ ACKNOWLEDGMENTS

This work was carried out primarily with funding and supports from the X10D Project (EC 287818) and The Leventis Foundation with support from EPSRC (EP/G037515/1 and EP/L016702/1). M.K. acknowledges support from Nanomatcell Project (EU 308997), and M.P. acknowledges support from the Artesun Project (EU 604397).

■ REFERENCES

(1) Ye, L.; Zhang, S. Q.; Zhao, W. C.; Yao, H. F.; Hou, J. H. *Chem. Mater.* **2014**, *26*, 3603.

(2) Hendriks, K. H.; Heintges, G. H. L.; Gevaerts, V. S.; Wienk, M. M.; Janssen, R. A. J. *Angew. Chem., Int. Ed.* **2013**, *52*, 8341.

(3) He, Z.; Zhong, C.; Su, S.; Xu, M.; Wu, H.; Cao, Y. *Nat. Photonics* **2012**, *6*, 591.

(4) Wu, J.-S.; Cheng, S.-W.; Cheng, Y.-J.; Hsu, C.-S. *Chem. Soc. Rev.* **2014**, DOI: 10.1039/C4CS00250D.

(5) Li, Y. *Acc. Chem. Res.* **2012**, *45*, 723.

(6) Guo, X.; Facchetti, A.; Marks, T. J. *Chem. Rev.* **2014**, *114*, 8943.

(7) Nielsen, C. B.; Turbiez, M.; McCulloch, I. *Adv. Mater.* **2013**, *25*, 1859.

(8) Small, C. E.; Chen, S.; Subbiah, J.; Amb, C. M.; Tsang, S.-W.; Lai, T.-H.; Reynolds, J. R.; So, F. *Nat. Photonics* **2012**, *6*, 115.

(9) Peet, J.; Kim, J. Y.; Coates, N. E.; Ma, W. L.; Moses, D.; Heeger, A. J.; Bazan, G. C. *Nat. Mater.* **2007**, *6*, 497.

(10) Mei, J.; Diao, Y.; Appleton, A. L.; Fang, L.; Bao, Z. *J. Am. Chem. Soc.* **2013**, *135*, 6724.

(11) Kim, G.; Kang, S.-J.; Dutta, G. K.; Han, Y.-K.; Shin, T. J.; Noh, Y.-Y.; Yang, C. *J. Am. Chem. Soc.* **2014**, *136*, 9477.

(12) Lee, J.; Han, A. R.; Yu, H.; Shin, T. J.; Yang, C.; Oh, J. H. *J. Am. Chem. Soc.* **2013**, *135*, 9540.

(13) Yan, H.; Chen, Z.; Zheng, Y.; Newman, C.; Quinn, J. R.; Dotz, F.; Kastler, M.; Facchetti, A. *Nature* **2009**, *457*, 679.

(14) Gao, J.; Dou, L. T.; Chen, W.; Chen, C. C.; Guo, X. R.; You, J. B.; Bob, B.; Chang, W. H.; Strzalka, J.; Wang, C.; Li, G.; Yang, Y. *Adv. Energy Mater.* **2014**, *4*, 1300739.

(15) Meager, I.; Ashraf, R. S.; Mollinger, S.; Schroeder, B. C.; Bronstein, H.; Beatrup, D.; Vezie, M. S.; Kirchartz, T.; Salleo, A.; Nelson, J.; McCulloch, I. *J. Am. Chem. Soc.* **2013**, *135*, 11537.

(16) Park, Y. S.; Wu, Q.; Nam, C.-Y.; Grubbs, R. B. *Angew. Chem., Int. Ed.* **2014**, *53*, 10691.

(17) Li, W.; Roelofs, W. S. C.; Turbiez, M.; Wienk, M. M.; Janssen, R. A. J. *Adv. Mater.* **2014**, *26*, 3304.

(18) Cho, M. J.; Shin, J.; Yoon, S. H.; Lee, T. W.; Kaur, M.; Choi, D. H. *Chem. Commun.* **2013**, *49*, 7132.

(19) Shahid, M.; McCarthy-Ward, T.; Labram, J.; Rossbauer, S.; Domingo, E. B.; Watkins, S. E.; Stingelin, N.; Anthopoulos, T. D.; Heeney, M. *Chem. Sci.* **2012**, *3*, 181.

(20) Shahid, M.; Ashraf, R. S.; Huang, Z. G.; Kronemeijer, A. J.; McCarthy-Ward, T.; McCulloch, I.; Durrant, J. R.; Sirringhaus, H.; Heeney, M. *J. Mater. Chem.* **2012**, *22*, 12817.

(21) Lee, J.; Han, A. R.; Kim, J.; Kim, Y.; Oh, J. H.; Yang, C. *J. Am. Chem. Soc.* **2012**, *134*, 20713.

(22) Kronemeijer, A. J.; Gili, E.; Shahid, M.; Rivnay, J.; Salleo, A.; Heeney, M.; Sirringhaus, H. *Adv. Mater.* **2012**, *24*, 1558.

(23) Bronstein, H.; Chen, Z. Y.; Ashraf, R. S.; Zhang, W. M.; Du, J. P.; Durrant, J. R.; Tuladhar, P. S.; Song, K.; Watkins, S. E.; Geerts, Y.; Wienk, M. M.; Janssen, R. A. J.; Anthopoulos, T.; Sirringhaus, H.; Heeney, M.; McCulloch, I. *J. Am. Chem. Soc.* **2011**, *133*, 3272.

(24) Bijleveld, J. C.; Verstrijden, R. A. M.; Wienk, M. M.; Janssen, R. A. J. *J. Mater. Chem.* **2011**, *21*, 9224.

(25) Bijleveld, J. C.; Karsten, B. P.; Mathijssen, S. G. J.; Wienk, M. M.; de Leeuw, D. M.; Janssen, R. A. J. *J. Mater. Chem.* **2011**, *21*, 1600.

(26) Jung, E. H.; Bae, S.; Yoo, T. W.; Jo, W. H. *Polym. Chem.* **2014**, *5*, 6545.

(27) Kaur, M.; Yang, D. S.; Shin, J.; Lee, T. W.; Choi, K.; Cho, M. J.; Choi, D. H. *Chem. Commun.* **2013**, *49*, 5495.

(28) McCormick, T. M.; Jahnke, A. A.; Lough, A. J.; Seferos, D. S. *J. Am. Chem. Soc.* **2012**, *134*, 3542.

(29) Detty, M. R.; O'Regan, M. B. In *Chemistry of Heterocyclic Compounds*; John Wiley & Sons, Inc.: Hoboken, NJ, 1994; p 1.

(30) Párkányi, C.; Aaron, J.-J. In *Theoretical and Computational Chemistry*; Cyril, P., Ed.; Elsevier: 1998; Vol. Vol. *5*, p 233.

(31) Fringuelli, F.; Taticchi, A.; Gronowitz, S.; Hörnfeldt, A.-B. *J. Heterocycl. Chem.* **1974**, *11*, 827.

(32) Jeffries-El, M.; Kobilka, B. M.; Hale, B. J. *Macromolecules* **2014**, *47*, 7253.

(33) Takimiya, K.; Kunugi, Y.; Konda, Y.; Niihara, N.; Otsubo, T. *J. Am. Chem. Soc.* **2004**, *126*, 5084.

(34) Bronstein, H.; Collado-Fregoso, E.; Hadipour, A.; Soon, Y. W.; Huang, Z. G.; Dimitrov, S. D.; Ashraf, R. S.; Rand, B. P.; Watkins, S. E.; Tuladhar, P. S.; Meager, I.; Durrant, J. R.; McCulloch, I. *Adv. Funct. Mater.* **2013**, *23*, 5647.

(35) Jahnke, A. A.; Howe, G. W.; Seferos, D. S. *Angew. Chem., Int. Ed.* **2010**, *49*, 10140.

(36) Sweat, D. P.; Stephens, C. E. *J. Organomet. Chem.* **2008**, *693*, 2463.

(37) Seitz, D. E.; Lee, S. H.; Hanson, R. N.; Bottaro, J. C. *Synth. Commun.* **1983**, *13*, 121.

(38) Tierney, S.; Heeney, M.; McCulloch, I. *Synth. Met.* **2005**, *148*, 195.

(39) Planells, M.; Schroeder, B. C.; McCulloch, I. *Macromolecules* **2014**, *47*, 5889.

(40) Sirringhaus, H. *Adv. Mater.* **2014**, *26*, 1319.

(41) Hendriks, K. H.; Li, W.; Wienk, M. M.; Janssen, R. A. *J. Am. Chem. Soc.* **2014**, *136*, 12130.

DOI: 10.1021/ja511984q
J. Am. Chem. Soc. 2015, 137, 1314−1321

(42) Liu, J.; Shao, S. Y.; Meng, B.; Fang, G.; Xie, Z. Y.; Wang, L. X.; Li, X. L. *Appl. Phys. Lett.* **2012**, *100*, 213906.
(43) Seo, J. H.; Gutacker, A.; Sun, Y.; Wu, H.; Huang, F.; Cao, Y.; Scherf, U.; Heeger, A. J.; Bazan, G. C. *J. Am. Chem. Soc.* **2011**, *133*, 8416.
(44) Zhou, H.; Zhang, Y.; Seifter, J.; Collins, S. D.; Luo, C.; Bazan, G. C.; Nguyen, T.-Q.; Heeger, A. J. *Adv. Mater.* **2013**, *25*, 1646.
(45) Liu, X.; Wen, W.; Bazan, G. C. *Adv. Mater.* **2012**, *24*, 4505.
(46) Lee, B. R.; Jung, E. D.; Nam, Y. S.; Jung, M.; Park, J. S.; Lee, S.; Choi, H.; Ko, S.-J.; Shin, N. R.; Kim, Y.-K.; Kim, S. O.; Kim, J. Y.; Shin, H.-J.; Cho, S.; Song, M. H. *Adv. Mater.* **2014**, *26*, 494.
(47) Lai, T. H.; Tsang, S. W.; Manders, J. R.; Chen, S.; So, F. *Mater. Today* **2013**, *16*, 424.
(48) Park, J. H.; Lee, T. W.; Chin, B. D.; Wang, D. H.; Park, O. O. *Macromol. Rapid Commun.* **2010**, *31*, 2095.

DOI: 10.1021/ja511984q
J. Am. Chem. Soc. 2015, 137, 1314−1321